REFERENCES

[1] G. Kantor "Direct contact microwave diathermy applicator," U.S. Patent 4 108 147, Aug. 22, 1978.

[2] G. Kantor and T. C. Cetas, "A comparative heating pattern study of direct contact applicators in microwave diathermy," *Radio Sci.*, vol. 12, no. 6 (S), pp. 111–120, Nov.–Dec. 1977.

[3] R. L. Magin and G. Kantor, "Comparison of the heating patterns of small microwave (2450 MHz) applicators," *J. Bioeng.* vol. 1, pp. 493–509, 1977.

[4] A. L. Van Koughnett and W. Wyslouzil, "A waveguide TEM mode exposure chamber," *J. Microwave Power*, vol. 7, no. 4, pp. 381–383, 1972.

[5] G. Kantor, D. M. Witters, and J. W. Greiser, "The performance of a new direct contact applicator for microwave diathermy," *IEEE Trans. Microwave Theory Tech.*, vol. MTT-26, pp. 563–568, Aug. 1978.

[6] H. I. Bassen, G. Kantor, P. S. Ruggera, and D. M. Witters, "Leakage in the proximity of microwave diathermy applicators used on humans and phantom models," HEW Publication (FDA) 79-8073, Oct. 1978.

[7] G. Kantor and D. M. Witters, "A new 915 MHz direct contact applicator with reduced leakage," *IEEE Trans. Microwave Theory Tech.*, submitted for publication.

[8] A. Y. Cheung, T. Dao, and J. E. Robinson, "Dual-beam TEM applicator for direct contact heating of dielectrically encapsulated malignancy mouse tumor," *Radio Sci.*, vol. 12, no. 6 (S), pp. 81–85, Nov.–Dec. 1977.

[9] T. C. Cetas and G. H. Nussbaum, "Physical aspects of hyperthermia," in *Progress in Medical Radiation Physics*. New York: Plenum, 1980.

A Novel Approach to the Design of Multiple-Probe High-Power Microwave Automatic Impedance Measuring Schemes

CHIA-LUN J. HU

Abstract—**Starting with a modified look at the phasor diagram of a multiple-probe system on a lossless waveguide, one can attain a geometrical method for designing various direct-reading microwave impedance-measuring schemes using fixed probes. This geometrical method will bypass a significant amount of algebraic complexity as encountered in classical algebraic methods. Hence it allows one to visualize the physical picture more clearly and guides one to modify the design more effectively to meet higher performance demands. This article reports a trend of design developments derived from this new point of view. It starts with the analysis of a two-probe system for measuring an unknown impedance $\bar{z}$. This is followed by modifications on the design guided by the new geometrical technique. Finally, two practical designs are derived for measuring an unknown microwave impedance automatically. One is to be used under fixed-frequency, swept-power conditions, and the other, under swept-frequency, swept-power conditions. These systems require only inexpensive low-frequency signal processors (either analog or digital) and fixed multiple probes. The output can be either analog with polar display or digital with accurate readouts. To the author's knowledge, these designs have not been derived in the past using multiple probes. A critical review on all multiple-probe systems reported in the literature is also discussed with their comparison to the present system.**

Manuscript received March 27, 1980; revised August 26, 1980. Patent application for the new designing method and the new schemes reported in this paper is in progress.

The author is with the Department of Electrical Engineering, University of Colorado, Boulder, CO 80309.

I. INTRODUCTION—BACKGROUND SURVEY

MULTIPLE PROBES mounted on a lossless waveguide terminated by an unknown impedance $\bar{z}$ have been used or proposed by many investigators to obtain data for calculating both phase and magnitude of the unknown complex $\bar{z}$. Samuel in 1947 [1] used two pairs of equidistant ($\lambda g/4$) probes interlaced by $\lambda g/8$ to measure and to display the impedance on an oscilloscope. He applied $V_1 - V_3$ and $V_2 - V_4$ to the vertical and horizontal inputs of an oscilloscope, respectively, where V_1, V_2, V_3, V_4 are square-law diode outputs from the probes. Although in his measurements the frequency was varied such that the impedance was traced as a curve on the oscilloscope, his scheme was actually derived from fixed-frequency assumptions. That is, he assumed that the angular distance between any adjacent probes is always kept at $\lambda g/8$

0018-9480/80/1200-1422$00.75

even when the frequency is swept. Ginzton reported in his book [2] an unpublished scheme used in 1945 by G. H. Taylor which is physically similar to Samuel's scheme—four equidistant probes separated by $\lambda g/8$. But he used the ratio of, not the difference between, the probe-detected outputs to calculate the $\bar{z}$. A chart was made for reading out the unknown $\bar{z}$ from these ratios detected at a fixed frequency. Duffin in 1952 [3] published still another similar scheme using three fixed probes separated by $\lambda g/8$. He then derived algebraically a set of equations for calculating the magnitude of $\bar{z}$ and the imaginary part of $\bar{z}$ from the probe detected data V_1/V_2 and V_3/V_2. Again, because of the restriction of $\lambda g/8$ between adjacent probes, this scheme is also restricted to fixed-frequency measurements. In 1952, King [4] generalized the Taylor's four-probe scheme by analyzing the ratio between the outputs V_1, V_2 of two fixed probes arbitrarily spaced. He proved algebraically that when this ratio is fixed, the trajectory of $\bar{z}$ on a Smith chart is a circle. He then derived a four-probe scheme which is quite similar to the one discussed in Ginzton's book. In 1962, Chamberlain *et al.* [5] proposed a scheme using three equidistant probes with arbitrary spacing between the probes. He then arrived at a set of equations for calculating $\bar{z}$ from the probe outputs at a fixed frequency. But when he proposed a signal-processing system to calculate the unknown $\bar{z}$ from the probe outputs, he missed a very important point—he neglected the phase distance between the loading point and the probes—which will lead to serious errors in the measurements. Hence, his scheme was never reported in the literature to show successful measurements. This point can be clearly seen from the geometrical method discussed in Section II when we design the fixed-frequency scheme.

Since 1962, there has been hardly any significant publication concerning multiple-probe schemes. A probable reason for this is that all the above investigators used algebraic methods to analyze the multiple-probe systems. These methods become very complicated when the probe separation is arbitrary and when the frequency is swept. Hence, most of these schemes are restricted to simple probe separations, for example, $\lambda g/8$. Consequently, most of these systems can only be used at a single "design frequency." On the other hand, we will see from Section II that the fixed-frequency scheme reported in this article is usable at any other fixed frequency after a simple calibration. The reason that this and other more versatile designs can be reached here is that a new method of design derived from a paper published by this author in 1979 [6] bypasses this mathematical difficulty and provides more perceptive pictures and easier ways to design the system. In the following, we will start with a modified look at the phasor analysis and from there we will derive a geometrical method, in contrast to the algebraic methods reported in the literature, for analyzing the $\bar{z}$ versus probe-output relations.

Finally, two new practical designs are described. One is a fixed- (but adjustable) frequency, swept-power $\bar{z}$ measuring scheme. The other, a swept-power, swept-frequency, $\bar{z}$ measuring scheme. Both can be used at low and high power levels.

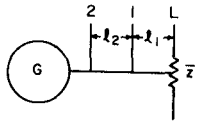

Fig. 1. A two-probe system for measuring $\bar{z}$.

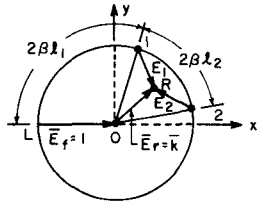

Fig. 2. Modified phasor diagram for Fig. 1.

II. Geometrical Approach and Fixed-Frequency, Swept-Power, Direct-Reading, $\bar{z}$ Measuring Scheme

If a lossless waveguide is connected between an unknown impedance $\bar{z}$ and a generator G, and if two fixed probes 1,2 are used to sample the E fields in the waveguide as shown in Fig. 1, then in principle, one can calculate both the magnitude and the phase of $\bar{z}$ from the sampled field strengths E_1, E_2 (or E_1^2, E_2^2 if square-law diodes are used) as shown in the modified phasor diagram of Fig. 2. In this figure, we have normalized the scale such that the forward-wave field in the waveguide is always represented by a unit-length phasor, and particularly, the forward field E_f at the loading point L is represented by the horizontal unit phasor $\overline{L0}$. Then, if the reflected field at the loading point is represented by $\overline{0R}$, we can keep $\overline{0R}$ fixed (in contrast to the conventional phasor analysis that one usually keeps the forward field $\overline{L0}$ fixed), and rotate $\overline{L0}$ clockwise to $\overline{10}$ with arc $L1$ equal to $2\beta l_1$ where βl_1 is the one-way phase difference between point 1 and point L in Fig. 1. The magnitude of the phasor $\overline{1R} \equiv \overline{10} + \overline{0R} \equiv$ (forward field + reflected field)$_{\text{at probe 1}}$ will then be equal to E_1 as detected by probe 1. Similarly, the magnitude of $\overline{2R}$ will be equal to E_2 as detected by probe 2. Now since points $L, 1, 2$ are fixed on the circle, and E_1, E_2 are measured, point R, or the reflected field $\overline{0R}$ at the loading point, can be determined geometrically.[1] This reflected field $\overline{0R}$ should be equal to the complex reflection coefficient $\bar{k}$ at the loading point since the forward field $\overline{L0}$ at the loading point is normalized to unity. Consequently, $\bar{k}$ at the loading point can be determined geometrically when E_1, E_2 are measured from the probe outputs. Now, if this phasor diagram is superimposed on a Smith chart with the chart scaled and oriented in such a way that the

[1]The geometrical problem here is the following. Given two fixed points 1, 2 and two fixed distances $1R \equiv E_1$, $2R \equiv E_2$, find the unknown point R. The way to solve this is to draw two circles with centers at points 1, 2 and radii E_1, E_2. The intersecting point R of these two circles is the unknown point R we want.

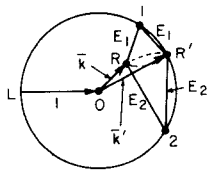

Fig. 3. Uniqueness ambiguity for the two-probe system.

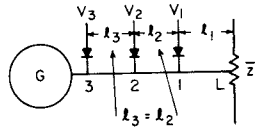

Fig. 4. A three-probe fixed-frequency $\bar{z}$ measuring scheme.

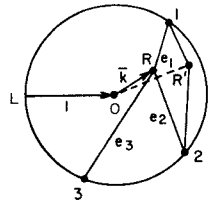

Fig. 5. Removal of the uniqueness ambiguity in the three-probe system.

circumference of Fig. 2 coincides with the circumference of the chart and the x–y coordinate[2] in Fig. 2 coincides with the rectangular coordinate in the Smith chart, then the $\bar{k}$ in Fig. 2 is just the $\bar{k}$ used in the Smith chart. Consequently, the impedance read off on the chart under point R (the tip of $\bar{k}$ in Fig. 2) will be equal to the unknown impedance $\bar{z}$ because the Smith chart is just a transformation from $\bar{k}$ to $\bar{z}$.

While this system for measuring $\bar{z}$ appears to be simple enough, there exists a uniqueness problem in the measurements. Two circles will generally intersect at two points and if the two intersecting points R and R' of the two intersecting circles happen to fall inside[3] the unit circle, as shown in Fig. 3, then two reflection coefficients $\bar{k}$ and $\bar{k}'$ or two possible unknown impedances $\bar{z}$ and $\bar{z}'$ will be obtained from only one set of probe outputs E_1, E_2. Consequently, this two-probe system may give double values for $\bar{z}$ under one set of measured probe data.

To remove this uniqueness ambiguity in the measurements, we can add a third probe to the system as shown in Fig. 4. The modified phasor diagram (similar to that of Fig. 2) for this three-probe system is shown in Fig. 5, where e_1, e_2, e_3 are the normalized total fields measured by probes 1, 2, and 3, respectively. (That is, $e_1 \equiv |\bar{E}_1/\bar{E}_f|$,

[2] x, y axes in Fig. 2 are the real and imaginary axes for expressing the complex number $\bar{k}$ because the unit phasor E_f (or $L0$) in Fig. 2 is along the positive x (real) direction. Hence E_f expressed in this x (real)–y (imaginary) coordinate is just $1+j0$, which is the reference phasor required for expressing the complex $\bar{k}$.

[3] If one intersecting point is inside the unit circle and one is outside, then the $\bar{k}$ corresponding to the one outside the unit circle will have a magnitude greater than unity which cannot be true for a passive load because $|\bar{k}|<1$ must hold for a passive load. Therefore, only the intersecting point inside the unit circle can give us correct $\bar{z}$, or the solution is unique only if *one* intersecting point is inside the circle.

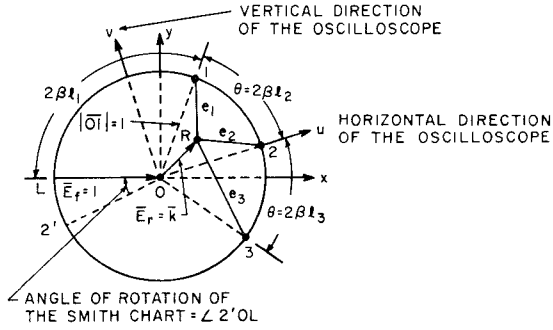

Fig. 6. Modified phasor diagram for calculating $\bar{z}$ from probe outputs e_1, e_2, e_3.

etc., and $\bar{E}_f$ is the forward field at the loading point.) We can see immediately now that the ambiguity of the double solutions in Fig. 3 does not exist here anymore. Because of the geometry of Fig. 5, we can see that a fixed-length e_3 will allow only one point to be selected from the double points R, R' shown in Fig. 3 for determining the unknown $\bar{k}$. That is, three fixed distances $1R \equiv e_1$, $2R \equiv e_2$, $3R \equiv e_3$ from three fixed points 1,2,3 will determine the position of the unknown point R uniquely in the plane.[4] Therefore, only one $\bar{k}$ or one $\bar{z}$ can be determined from one set of probe outputs e_1, e_2, e_3.

Now we would like to make a practical design based on this three-probe system. That is, we would like first to calculate $\bar{k}$ at the loading point analytically in terms of e_1, e_2, e_3 and then to design some signal processors to carry out this calculation and transform this calculated $\bar{k}$ into $\bar{z}$ automatically. In the following, we will first calculate the components of $\bar{k}$ in terms of e_1, e_2, e_3 using some geometrical means. To simplify the calculation, let us assume that $l_2 = l_3$ in Fig. 4 such that in the modified phasor diagram of Fig. 6, arc $12 =$ arc $23 \equiv \theta$. Let us then draw a rectangular coordinate axes U–V with $\overline{0U}$ coinciding with $\overline{02}$ as shown in Fig. 6. Then the components k_u, k_v of $\bar{k}$ expressed in this coordinate system can be calculated from e_1, e_2, e_3 by noting that the vector equation $\bar{A}-\bar{B}=\bar{C}$ is equivalent to the algebraic equation $(A_u-B_u)^2+(A_v-B_v)^2=|C|^2$. With this equation, we see that the three vector equations $\overline{01}-\overline{0R}=\overline{R1}, \overline{02}-\overline{0R}=\overline{R2}, \overline{03}-\overline{0R}=\overline{R3}$ shown in Fig. 6 are equivalent to the following algebraic equations, respectively:

$$(\cos\theta-k_u)^2+(\sin\theta-k_v)^2=e_1^2 \tag{1}$$

$$(1-k_u)^2+k_v^2=e_2^2 \tag{2}$$

$$(\cos\theta-k_u)^2+(-\sin\theta-k_v)^2=e_3^2. \tag{3}$$

k_u, k_v can then be solved by applying the operations (1)+(3)−2(2), and (3)−(1) to these equations, with the

[4] There must, of course, exist a certain restraint among e_1, e_2, e_3 because this is an overdetermined system. Three fixed distances from three fixed points are actually more than those required to determine the position of the unknown point R in the plane. But this "oversupply" of data will remove the double-solution ambiguity as shown in Fig. 5.

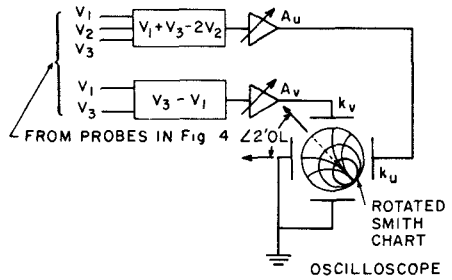

Fig. 7. A practical three-probe system for automatic $\bar{z}$ measurements at fixed frequencies.

following:

$$k_u = \frac{e_1^2 + e_3^2 - 2e_2^2}{4(1-\cos\theta)} = A_u(V_1 + V_2 - 2V_3) \tag{4}$$

$$k_v = \frac{e_3^2 - e_1^2}{4\sin\theta} = A_v(V_3 - V_1) \tag{5}$$

where $V_i \sim e_i^2$ are the square-law diode outputs from the probes and A_u, A_v are two proportional constants if θ or the frequency $f(\theta \equiv 2\beta l = (4\pi l/V_g)f)$ is kept unchanged in the measurements.

Now if we design two signal processors to process the probe outputs V_1, V_2, V_3 according to (4), (5), and if the output voltages k_u, k_v of these two processors are connected, respectively, to the horizontal and the vertical inputs of an oscilloscope as shown in Fig. 7, then the displacement of the beam spot on the scope will be proportional to phasor $\overline{0R} \equiv \bar{k}$ in Fig. 6 when $\overline{0U}, \overline{0V}$ in Fig. 6 are taken, respectively, as the horizontal and the vertical directions of the scope. Thus with a proper calibration and with a Smith chart properly oriented and overlayed on the scope, we can use this displayed $\bar{k}$ to read the unknown $\bar{z}$ directly from the Smith chart. Notice that it is $\overline{L0}$, or $\overline{0X}$, not $\overline{0U}$, in Fig. 6 that must coincide with the horizontal axis of the Smith chart, because $\overline{0R}$, or the reflected field $\bar{E}_r$ at the loading point, can be taken as $\bar{k}$ only when $\overline{L0}$, or the forward field $\bar{E}_f$ at the loading point, is taken as unity as shown in Fig. 6. Therefore, $\bar{z}$ can be read off directly from the Smith chart overlay only when this chart is rotated from the horizontal axis $\overline{0U}$ by an angle equal to $\angle 2'0L$ as shown in both Figs. 6 and 7.[5]

To calibrate this system, we need to connect a sliding short to the loading point L of Fig. 4. We can then adjust the amplifier gains A_u, A_v in Fig. 7 such that when the system is in calibration, the beam spot on the scope will trace a curve exactly along the circumference of the Smith chart as the sliding short is moved in and out. This is so because $\bar{z}=0$ on the Smith chart is equivalent to point L in Fig. 6 ($\bar{z}=0$ means that $\bar{E}_r = -\bar{E}_f$ or point R coincides with point L in Fig. 6) and adjustment of the sliding short is equivalent to the adjustment of $\angle 2\beta l_1$ in Fig. 6. This, in turn, is equivalent to the adjustment of the angle of rotation of the Smith chart or adjustment of $\angle 2'0L \equiv \pi - \theta - 2\beta l_1 = \text{constant} - 2\beta l_1$. Consequently, when the chart is fixed in place, adjustment of the sliding short will move the beam spot along the circumference of the Smith chart if the system is in calibration.

Notice that after this calibration process, we do not have to normalize the probe outputs against the forward field $\bar{E}_f$ if the output power of the generator is very stable. However, if the generator output power is not stable, such that the forward field at the loading point during calibration is not the same as that during the $\bar{z}$ measurements, or, if we intend to sweep the power level for nonlinear $\bar{z}$ measurements, then we need to normalize the probe outputs. That is, we should use a directional coupler (or a magic T as used in the swept-frequency scheme discussed later in Section III) to sample the forward field $\bar{E}_f$ or the square of the forward field $E_f^2 \sim V_f$ if a square-law diode is used. We should then use this V_f to divide all probe outputs V_1, V_2, V_3 by means of analog dividers. The outputs of these dividers are then the "normalized" probe outputs which should be constants and not be affected by power fluctuation or sweeping of the power level when $\bar{z}$ and frequency are unchanged. Consequently, the $\bar{z}$ measurements will not depend on the power level when these normalized probe outputs are used. The system can then be used as a swept-power, fixed-frequency, direct-reading, $\bar{z}$ measuring scheme reusable at any fixed frequencies.[6]

III. Swept-Frequency, Swept-Power, Direct-Reading, Impedance-Measuring Scheme

If we can express components k_x, k_y [where x, y are the horizontal (real) and the vertical (imaginary) axes of the Smith chart] of the loading point reflection coefficient $\bar{k}$ in terms of the probe outputs e_i *independent* of θ or frequency $f(\theta \equiv (4\pi l/V_g)f)$, then we can design two signal processors to calculate these k_x, k_y in terms of the probe outputs e_i. The outputs k_x, k_y of these processors can then be applied, respectively, to the horizontal and the vertical inputs of an oscilloscope. A Smith chart can be overlayed on the scope in such a way that x, y axes of the Smith chart coincide with the horizontal and the vertical directions of the scope, respectively. The beam spot on the Smith chart will then indicate automatically the value of the complex $\bar{z}$ *at any frequency* f if the scope is properly calibrated. Consequently, in order to build a swept-frequency $\bar{z}$ measuring scheme, we need to modify the probe arrangement such that k_x, k_y can be expressed directly as functions of probe outputs independent of the frequency. To eliminate this frequency dependence, we

[5] Chamberlain's scheme discussed in the Introduction (Section I) is very similar to the three-probe scheme discussed here. His equations (6), (7) are exactly the same as (4), (5) derived here, except that he did not take the phase distance between the loading point and the central probe into account. This phase distance is equal to $2\beta(l_1+l_2) = \pi - \angle 2'0L$ in Fig. 6 here, and $\angle 2'0L$ is the angle of rotation of the Smith chart as described in the text. Consequently, Chamberlain's proposed scheme (never carried out experimentally) *would not work* in general for correct measurements of $\bar{z}$ if the rotation of the Smith chart were not carried out.

[6] When frequency changes, θ or the proportional constants A_u, A_v in (4), (5) will change. Therefore, a recalibration of the system by varying the amplifier gains A_u, A_v in Fig. 7 must be carried out for correct z measurements at this new frequency.

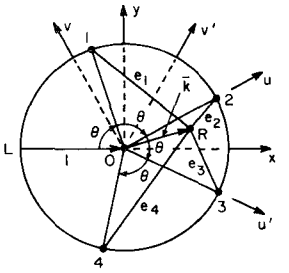

Fig. 8. Modified phasor diagram for the four-probe swept-frequency scheme.

can add a fourth equidistant probe to the three-probe system previously discussed and obtain from the probe outputs e_2, e_3, e_4 another set of equations similar to (4), (5). If θ can be eliminated from these two sets of equations, the components of $\bar{k}$ can be expressed directly in terms of outputs e_1, e_2, e_3, e_4 of these probes without going through θ or f. The following design analysis is based on this point of view.

First, we notice that in the modified phasor diagram (Fig. 8), $L1 = 12 = 23 = 24 = 34 = \theta$ because of the equidistance probes we used. Let us then define two rectangular coordinate systems U–V and U'–V' such that $\overline{0U}$ coincides with $\overline{02}$ and $\overline{0U'}$ coincides with $\overline{03}$ as shown in Fig. 8. Then as we have seen, expressed in the U–V coordinate system, components k_U, k_V of $\bar{k}$ at the loading point are functions of e_1, e_2, e_3, and θ shown by (4), (5). Similarly expressed in the u'–v' coordinate, components k'_u, k'_v of $\bar{k}$ can be calculated by the following equations which are obtained from (4), (5) by replacing indices 1,2,3 with 2,3,4:

$$k'_u = \frac{e_2^2 + e_4^2 - 2e_3^2}{4(1-\cos\theta)} \tag{6}$$

$$k'_v = \frac{e_4^2 - e_2^2}{4\sin\theta}. \tag{7}$$

Now since k_u, k_v and k'_u, k'_v are related by a rotation of coordinates implemented by the following equations:

$$k'_u = k_u\cos\theta - k_v\sin\theta \tag{8}$$

$$k'_v = k_u\sin\theta + k_v\cos\theta. \tag{9}$$

The angle θ, or $\cos\theta$, can be solved in terms of e_1, e_2, e_3, e_4 by substituting (4)–(6) into (8). Therefore, k_u, k_v in (4), (5) can be expressed in terms of e_1, e_2, e_3, e_4 only, independently of θ. These k_u, k_v can be rotated to k_x, k_y in the x–y coordinate (the Smith chart coordinate) by the following equations of rotation, with angle of rotation equal to $\pi - 2\theta$ as shown in Fig. 8:

$$k_x = -k_u\cos 2\theta - k_v\sin 2\theta \tag{10}$$

$$k_y = k_u\sin 2\theta - k_v\cos 2\theta. \tag{11}$$

Then we have k_x, k_y, the real and imaginary components of $\bar{k}$ at the loading point expressed *explicitly* in terms of probe outputs e_i *independent of* θ *or frequency* f as shown by the equation set (9) below:

$$k_x = k_u(1-2\cos^2\theta) - \frac{e_3^2 - e_1^2}{2}\cos\theta \tag{9-1}$$

$$k_y = 2k_u\sin\theta\cos\theta + \frac{e_3^2 - e_1^2}{4\sin\theta}(1-2\cos^2\theta) \tag{9-2}$$

where

$$k_u \equiv \frac{e_1^2 + e_3^2 - 2e_2^2}{4(1-\cos\theta)} \tag{9-3}$$

$$\cos\theta \equiv \frac{e_1^2 + e_3^2 - e_2^2 - e_4^2}{2(e_2^2 - e_3^2)} \tag{9-4}$$

and

$$\sin\theta = \sqrt{1-\cos^2\theta}\ . \tag{9-5}$$

It then appears to us that these equations may be used directly to design signal processors for calculating k_x, k_y from e_1, e_2, e_3, e_4 in a swept-frequency $\bar{z}$ measuring scheme. But unfortunately there again exist three practical problems. First, actually there should be $\pm$ signs in front of the square root of (9-5), or uniqueness ambiguity may again arise. Second, when $\sin\theta$ in (9-2) or $(1-\cos\theta)$ in (9-3) equals zero, the mathematical expression becomes indefinite and not suitable for any signal processors. Third, when $e_2 = e_3$, $\cos\theta$ in (9-4) becomes indeterminable. However, all these difficulties can be overcome as explained in the following.

First, if we choose the separation l between the adjacent probes *short* enough such that $0 < \theta < \pi$ when frequency is swept in the designated frequency range of the waveguide, then $\sin\theta$ is always positive and greater than zero. Therefore the "+" sign of (9-5) should always be chosen as shown. Also $\sin\theta$ and $(1-\cos\theta)$ will never be equal to zero so that the second handicap will not occur under this choice of l. As to the third difficulty, we see from the geometry in Fig. 8, that if $e_2 = e_3$, R point is on the dividing line of $\angle 203$, or $\angle 104$. Therefore, $e_1 = e_4$ must also follow. Consequently, (9-4) becomes an indeterminant form of 0/0. This is not suitable for any signal processor. But it can be overcome by the following modification. Suppose we add still another equidistance probe, probe 5, to the system as shown in the upper part of Fig. 9, then when $e_2 = e_3$ occurs, we can calculate θ from the outputs of e_2 to e_5 instead of e_1 to e_4. Because by the geometry of Fig. 8, if R happens to fall on the dividing line of $\angle 203$, it will never fall on the dividing line of $\angle 304$. Therefore, $e_3 \neq e_4$ and $\cos\theta$ can be calculated by

$$\cos\theta = \frac{e_2^2 + e_4^2 - e_3^2 - e_5^2}{2(e_3^2 - e_4^2)}$$

instead of that given by (9-4). This switching action can be implemented by the comparator and the analog switches shown in the lower part of Fig. 9. When $e_2 - e_3$ approaches zero, the comparator will yield an output signal "high" to activate all the analog switches such that

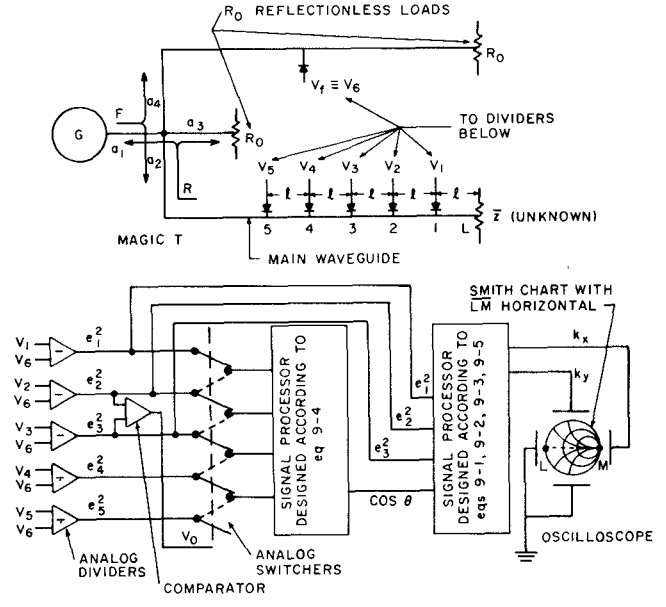

Fig. 9. A practical system for automatic $\bar{z}$ measurements at swept frequencies and swept powers.

the $\cos\theta$ processor will process the inputs from e_2 to e_5 instead of e_1 to e_4. The rest of the calculation or the data processing are straightforward by following the other four equations in (9). The outputs k_x, k_y of the second processor in Fig. 9 can then be directly connected to the display oscilloscope as shown in the lower part of Fig. 9 where the x axis or $\overline{LM}$ in the Smith chart is set such that it coincides with the horizontal axis of the oscilloscope. This is a system capable of measuring $\bar{z}$ automatically when frequency f is swept, because after a proper calibration, the displacement of the beam spot on the scope is equal to the $\bar{k}$ at the loading point under any frequency. Therefore, the $\bar{z}$ at any swept frequency can be read off directly from the Smith chart.

To calibrate the system, we should first understand the normalization process used in the system. The magic T and probe 6 in the upper part of Fig. 9 are used for normalizing the probe outputs as explained in the following. The forward wave F coming from the generator will be divided equally between arms a_2, a_4 of the magic T, but the reflected wave R from a_2 arm will not go into a_4 because of the scattering property of the magic T. Hence $V_6 \equiv V_f$ will *indirectly* monitor the forward wave in the main guide. Consequently, V_6 can be used to normalize all probe outputs in the main guide by analog dividers as shown in the lower part of Fig. 9. A directional coupler is not recommended for monitoring the forward wave because its frequency response does not match that of the probes when the frequency is swept. On the other hand, the frequency response of V_6 in arm a_4 shown in Fig. 9 should be exactly the same as those of V_1 to V_5 in arm a_2 because of the geometrical symmetry of the magic T. Therefore, the normalization process here should be quite independent of the frequency as well as the power when the frequency or the power is swept. Consequently Fig. 9 is a swept-frequency, swept-power, direct-reading, $\bar{z}$ measuring scheme.

To calibrate the system, we need to use a reflectionless load connected to the loading point and adjust the probe sensitivities as well as the divider amplification factors, such that they are all the same for all probes and all dividers. Then we should connect a short plate to the loading point and adjust the gains of the two signal processors such that the beam spot on the scope is brought to point L or $\bar{z}=0$ point on the Smith chart. This will then complete the calibration of the system.

The signal processors implementing equations (9-1) to (9-5) should not be very complicated because only $\sqrt{\ }, +, -, \times, \div$ are involved. Either digital or analog processors can be used to implement these equations. Digital displays instead of polar-display oscilloscopes can also be used to read out $\bar{k}$ or $\bar{z}$ accurately. The main factor that may affect the accuracy of the measurements should be the dc signal processors used here because the mechanical and the microwave structures of this system are quite simple and quite symmetric. Probe-loading and probe-coupling effects should not be a problem here because the coupling can be made very slight due to high power level used.

IV. Discussion and Conclusion

From a mathematical point of view, generally, n equations are sufficient for solving n unknowns with possible multiple roots. Therefore, two equations derived from two fixed-probe outputs e_1, e_2 should be adequate to solve two unknowns k_x, k_y at a fixed frequency. But not only is it difficult to implement k_x, k_y algebraically from the probe outputs e_1, e_2 but also, as it is shown in Fig. 3, double solutions occur. Therefore, we add a third equation derived from a third probe added to the system for eliminating this mathematical difficulty as well as the double-root ambiguity as explained in Section II. On the other hand, this three-probe system is actually an overdetermined system as explained in footnote no. 4. Therefore, in principle, three unknowns, k_x, k_y, and θ should be solvable from the three equations (1)–(3) in terms of e_1, e_2, e_3 which would suggest that we could build a swept-frequency scheme using only three probes. But, in reality, θ is again very difficult to solve from (1)–(3), and again, multiple roots occur. Therefore, we add a fourth equation derived from a fourth probe for solving the three unknowns k_x, k_y, θ in terms of e_1, e_2, e_3, e_4. The trend of development is such that, using the present geometrical method, we can see clearly where the uniqueness ambiguities arise and where the algebraic difficulties lie. Furthermore, we can also see easily from this geometrical method how to overcome these ambiguities and these algebraic difficulties by adding more and more probes to the system. That is, we can use the "oversupply" of probe detected data to "trade off" these design problems when higher and higher system performances are demanded. These "tradeoff" advantages may be very difficult to discover if one uses

algebraic methods alone. This may be the main advantage of the present geometrical method.

As reported here, following this geometrical method, two practical systems for automatic measurements of $\bar{z}$ are designed here. One can be used under fixed but adjustable frequency, swept-power conditions, and the other, under swept-frequency, swept-power conditions. The bandwidths of both these systems should be about the same as those of the waveguides themselves if the probe loading is very slight. These systems can be used in either high-power or low-power levels as long as the probes can pick up enough signals without loading the waveguide. Also following this new method, further generalization of the system may be reached. For example, we may use different probe arrangements on a "loop line" for measuring the transfer functions or the scattering matrix of an unknown microwave component, or, we may use more probes to check and to enhance the measurement accuracy.

References

[1] A. L. Samuel, "An oscillographic method of presenting impedance on a reflection-coefficient plane," *Proc. IRE*, vol. 35, pp. 1279–1283, Nov. 1947.

[2] E. L. Ginzton, *Microwave Measurements*. New York: McGraw-Hill, 1957, pp. 303–307.

[3] W. J. Duffin, "Three probe method of impedance measurement," *Wireless Eng.*, pp. 317–320, Dec. 1952.

[4] D. D. King, *Measurements at Centimeter Wavelength*. Princeton, NJ: Van Nostrand, 1952, pp. 197–201.

[5] J. K. Chamberlain and B. Easter, "A technique for the continuous indication of waveguide reflection coefficient, impedance, or admittance," *Proc. Inst. Elec. Eng.*, pp. 696–703, May 1962.

[6] C. J. Hu, "On-line measurements of the fast changing dielectric constant in oil shale due to high power microwave heating," *IEEE Trans. Microwave Theory Tech.*, vol. MTT-27, pp. 38–43, Jan. 1979.

Corporate and Tandem Structures for Combining Power from 3^N and $2N+1$ Oscillators

SHIZUO MIZUSHINA, MEMBER, IEEE, HIROSHI KONDOH, AND MITSUAKI ASHIKI

Abstract—**The output power from three Gunn oscillators was combined using a short-slot coupler in conjunction with high-level injection locking with the power combining efficiency of about 100 percent at 9.7 GHz. Using the 3-oscillator structure as the building block, we constructed $(3^2=)$9-oscillator corporate structure and $(2\times4+1=)$9- and $(2\times6+1=)$13-oscillator tandem structures to demonstrate power combining efficiencies of 92, 95, and 93 percent, respectively, at 9.6 GHz.**

Introduction

VARIOUS TECHNIQUES for combining power from microwave solid-state sources have been described by many authors over the years [1]–[9]. Some of the techniques, most notably, the single-cavity-multiple-device techniques reported by Kurokawa and Magalhaes [2] and by Harp and Stover [3], have gained practical importance to fulfill a class of communication and radar transmitter requirements during the last several years. Nevertheless, it is always interesting to explore new high-efficiency power combining techniques that would offer possibilities of achieving higher power at higher frequencies. This paper describes a new method of combining power from multiple oscillators using short-slot couplers [10] in conjunction with high-level injection locking.

Manuscript received April 15, 1980; revised July 22, 1980.

S. Mizushina and M. Ashiki are with The Research Institute of Electronics, Shizuoka University, Hamamatsu 432, Japan.

H. Kondoh is with the School of Electrical Engineering, Cornell University, Ithaca, NY 14853.

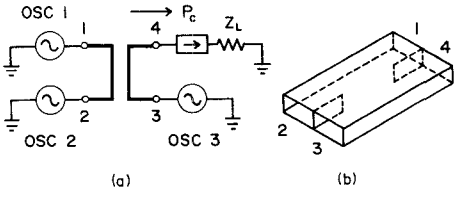

Fig. 1. (a) A 3-oscillator structure using a hybrid coupler. (b) A short-slot coupler used in the present work.

Principles

Three identical oscillators and a matched load are connected to a four-port hybrid coupler to form a 3-oscillator structure, as shown in Fig. 1(a), which is the building block of our power combining structures. The coupler

0018-9480/80/1200-1428$00.75 ©1980 IEEE